V European Conference on Computational Fluid Dynamics
ECCOMAS CFD 2010
J. C. F. Pereira and A. Sequeira (Eds)
Lisbon, Portugal,14-17 June 2010

# DGFEM FOR THE NUMERICAL SOLUTION OF COMPRESSIBLE FLOW IN TIME DEPENDENT DOMAINS AND APPLICATIONS TO FLUID-STRUCTURE INTERACTION[1]

**Miloslav Feistauer*, Jan Česenek*, Jaromír Horáček†, Václav Kučera*, Jaroslava Prokopová*** [1]

*Charles University Prague,
Faculty of Mathematics and Physics,
186 75 Sokolovska 83, Prague,
Czech Republic,
e-mail: feist@karlin.mff.cuni.cz
†Institute of Thermomechanics,
Academy of Sciences of Czech Republic,
Dolejškova 5, 182 00 Praha 8,
Czech Republic,
e-mail: jaromirh@it.cas.cz

**Key words:** compressible Euler and Navier-Stokes equations, time dependent domain, ALE method, discontinuous Galerkin method, semi-implicit time discretization, boundary conditions, shock indicator, artificial viscosity, flow in a channel with moving walls, flow induced airfoil vibrations

**Abstract.** *The paper is concerned with the simulation of inviscid and viscous compressible flow in time dependent domains. The motion of the boundary of the domain occupied by the fluid is taken into account with the aid of the ALE (Arbitrary Lagrangian-Eulerian) formulation of the Euler and Navier-Stokes equations describing compressible flow. They are discretized by the discontinuous Galerkin finite element method using piecewise polynomial discontinuous approximations. The time discretization is based on a semi-implicit linearized scheme, which leads to the solution of a linear algebraic system on each time level. Moreover, we use special treatment of boundary conditions and shock capturing, allowing the solution of flow with a wide range of Mach numbers. As a result we get an efficient and robust numerical process. The applicability of the developed method will be demonstrated by computational results obtained for compressible inviscid and viscous flow in channels with moving walls and flow induced airfoil vibrations.*

[1]This work is a part of the research project MSM 0021620839 financed by the Ministry of Education of the Czech Republic and was partly supported by the Grant No. 201/08/0012 of the Czech Science Foundation. The research of J. Horáček was supported by the project OC 09019 of the Ministry of Education of the Czech Republic. .

## 1 Introduction

The interaction of fluid flow with vibrating bodies plays a significant role in many areas of science and technology. We mention, for example, development of airplanes (vibrations of wings) or turbines (blade vibrations), some problems from civil engineering (interaction of wind with constructions as bridges, TV towers or cooling towers of power stations), car industry (vibration of various elements of a carosery), but also in medicine (hemodynamics or flow in the glottis with vibrating vocal folds). In a number of these examples the moving medium is a gas, i.e. compressible flow. For low Mach number flows incompressible models are used (as e.g. in [16]), but in some cases compressibility plays an important role.

The solution of fluid-structure interaction requires the coupling of the solution of equations describing the fluid flow with equations describing the structural behaviour. Due to the deformation and/or vibrations of structures, the computational domain is time dependent. There exist several techniques of the solution of incompressible flow in time dependent domains. See, e.g. [16] and references therein. The numerical simulation of compressible flow is much more difficult, particularly in time dependent domains. It is necessary to overcome difficulties caused by nonlinear convection dominating over diffusion, which leads to boundary layers and wakes for large Reynolds numbers and shock waves and contact discontinuities for high Mach numbers and instabilities caused by acoustic effects for low Mach numbers.

It appears that a suitable numerical method for the solution of compressible flow is the discontinuous Galerkin finite element method (DGFEM). It employs piecewise polynomial approximations without any requirement on the continuity on interfaces between neighbouring elements. The DGFEM was used for the numerical simulation of the compressible Euler equations, for example, by Bassi and Rebay in [1], where the space DG discretization was combined with explicit Runge-Kutta time discretization. In [2] Baumann and Oden describe an *hp* version of the space DG discretization with explicit time stepping to compressible flow. Van der Vegt and van der Ven apply space-time discontinuous Galerkin method to the solution of the Euler equations in [17], where the discrete problem is solved with the aid of a multigrid accelerated pseudo-time-integration. The papers [7] and [9] are concerned with a semi-implicit DGFEM technique for the solution of inviscid compressible flow, which is unconditionally stable. In [11], this method was extended so that the resulting scheme is robust with respect to the magnitude of the Mach number. The paper [6] is concerned with discontinuous Galerkin method for viscous compressible flow.

The goal of our research is the numerical simulation of interaction of compressible flow with structures as, e.g. flow induced airfoil vibrations or the flow past an elastic wall vibrating due to the influence of an airflow. We are concerned with the generalization of the method from [11], [9] and [6] to the solution of compressible inviscid and viscous flow in time dependent domains. The main ingredients of the method is the discontinuous Galerkin space semidiscretization of the Euler equations written in the ALE (arbi-

trary Lagrangian-Eulerian) form, semi-implicit time discretization, suitable treatment of boundary conditions and the shock capturing avoiding Gibbs phenomenon at discontinuities. Numerical experiments prove the applicability of the method. The applicability of the developed technique is demonstrated by some numerical experiments.

## 2 Formulation of the problem

We shall be concerned with the numerical solution of compressible flow in a bounded domain $\Omega_t \subset I\!R^2$ depending on time $t \in [0,T]$. Let the boundary of $\Omega_t$ consist of three different parts: $\partial\Omega_t = \Gamma_I \cup \Gamma_O \cup \Gamma_{W_t}$, where $\Gamma_I$ is the inlet, $\Gamma_O$ is the outlet and $\Gamma_{W_t}$ denotes impermeable walls that may move in dependence on time.

The system describing compressible flow consisting of the continuity equation, the Navier-Stokes equations and the energy equation can be written in the form

$$\frac{\partial \boldsymbol{w}}{\partial t} + \sum_{s=1}^{2} \frac{\partial \boldsymbol{f}_s(\boldsymbol{w})}{\partial x_s} = \sum_{s=1}^{2} \frac{\partial \boldsymbol{R}_s(\boldsymbol{w}, \nabla \boldsymbol{w})}{\partial x_s}, \tag{1}$$

where

$$\begin{aligned}
\boldsymbol{w} &= (w_1, \dots, w_4)^{\mathcal{T}} = (\rho, \rho v_1, \rho v_2, E)^{\mathcal{T}} \in I\!R^4, \\
\boldsymbol{w} &= \boldsymbol{w}(x,t),\ x \in \Omega_t,\ t \in (0,T), \\
\boldsymbol{f}_i(\boldsymbol{w}) &= (f_{i1}, \cdots, f_{i4})^{\mathcal{T}} = (\rho v_i, \rho v_1 v_i + \delta_{1i}\, p, \rho v_2 v_i + \delta_{2i}\, p, (E+p) v_i)^{\mathcal{T}}, \\
\boldsymbol{R}_i(\boldsymbol{w}, \nabla \boldsymbol{w}) &= (R_{i1}, \dots, R_{i4})^{\mathcal{T}} = \left(0, \tau_{i1}^V, \tau_{i2}^V, \tau_{i1}^V\, v_1 + \tau_{i2}^V\, v_2 k \partial\theta/\partial x_i\right)^{\mathcal{T}}, \\
\tau_{ij}^V &= \lambda\, \mathrm{div}\boldsymbol{v}\, \delta_{ij} + 2\mu\, d_{ij}(\boldsymbol{v}),\ d_{ij}(\boldsymbol{v}) = \frac{1}{2}\left(\frac{\partial v_i}{\partial x_j} + \frac{\partial v_j}{\partial x_i}\right).
\end{aligned} \tag{2}$$

We use the following notation: $\rho$ – density, $p$ – pressure, $E$ – total energy, $\boldsymbol{v} = (v_1, v_2)$ – velocity, $\theta$ – absolute temperature, $\gamma > 1$ – Poisson adiabatic constant, $c_v > 0$ – specific heat at constant volume, $\mu > 0, \lambda = -2\mu/3$ – viscosity coefficients, $k$ – heat conduction. The vector-valued function $\boldsymbol{w}$ is called state vector, the functions $\boldsymbol{f}_i$ are the so-called inviscid fluxes and $\boldsymbol{R}_i$ represent viscous terms.

The above system is completed by the thermodynamical relations

$$p = (\gamma - 1)(E - \rho|\boldsymbol{v}|^2/2), \quad \theta = \left(\frac{E}{\rho} - \frac{1}{2}|\boldsymbol{v}|^2\right)/c_v. \tag{3}$$

The complete system is equipped with the initial condition

$$\boldsymbol{w}(x,0) = \boldsymbol{w}^0(x), \quad x \in \Omega_0, \tag{4}$$

and the following boundary conditions:

$$\text{a)}\ \ \rho|_{\Gamma_I} = \rho_D, \quad \text{b)}\ \ \boldsymbol{v}|_{\Gamma_I} = \boldsymbol{v}_D = (v_{D1}, v_{D2})^{\mathrm{T}}, \tag{5}$$

$$\text{c)}\ \ \sum_{i,j=1}^{2} \tau_{ij}^V n_i v_j + k\frac{\partial \theta}{\partial n} = 0 \quad \text{on } \Gamma_I, \tag{6}$$

$$\text{a)}\ \ \boldsymbol{v}|_{\Gamma_{W_t}} = \boldsymbol{z}_D = (z_{D1}, z_{D2}) - \text{ velocity of a moving wall}, \quad \text{b)}\ \ \frac{\partial \theta}{\partial n}|_{\Gamma_{W_t}} = 0 \text{ on } \Gamma_{W_t}, \tag{7}$$

$$\text{a)}\ \ \sum_{i=1}^{2} \tau_{ij}^V n_i = 0, \quad j = 1,\, 2, \quad \text{b)} \frac{\partial \theta}{\partial n} = 0 \text{ on } \Gamma_O. \tag{8}$$

In order to treat the time dependence of the domain, we use the so-called *arbitrary Lagrangian-Eulerian* ALE technique, proposed in [13]. We define a reference domain $\Omega_0$ and introduce a regular one-to-one ALE mapping of $\Omega_0$ onto $\Omega_t$ (cf. [13], [16] and [17])

$$\mathcal{A}_t : \overline{\Omega}_0 \longrightarrow \overline{\Omega}_t,\ i.e.\ \boldsymbol{X} \in \overline{\Omega}_0 \longmapsto \boldsymbol{x} = \boldsymbol{x}(\boldsymbol{X}, t) = \mathcal{A}_t(\boldsymbol{X}) \in \overline{\Omega}_t.$$

Here we use the notation $\boldsymbol{X}$ for points in $\overline{\Omega}_0$ and $\boldsymbol{x}$ for points in $\overline{\Omega}_t$.

Further, we define the domain velocity:

$$\tilde{\boldsymbol{z}}(\boldsymbol{X}, t) = \frac{\partial}{\partial t}\mathcal{A}_t(\boldsymbol{X}), \quad t \in [0, T],\ \boldsymbol{X} \in \Omega_0,$$
$$\boldsymbol{z}(\boldsymbol{x}, t) = \tilde{\boldsymbol{z}}(\mathcal{A}^{-1}(\boldsymbol{x}), t), \quad t \in [0, T],\ \boldsymbol{x} \in \Omega_t$$

and the ALE derivative of a function $f = f(\boldsymbol{x}, t)$ defined for $\boldsymbol{x} \in \Omega_t$ and $t \in [0, T]$:

$$\frac{D^A}{Dt} f(\boldsymbol{x}, t) = \frac{\partial \tilde{f}}{\partial t}(\boldsymbol{X}, t), \tag{9}$$

where

$$\tilde{f}(\boldsymbol{X}, t) = f(\mathcal{A}_t(\boldsymbol{X}), t),\ \boldsymbol{X} \in \Omega_0,\ \boldsymbol{x} = \mathcal{A}_t(\boldsymbol{X}).$$

As a direct consequence of the chain rule we get the relation

$$\frac{D^A f}{Dt} = \frac{\partial f}{\partial t} + \operatorname{div}(\boldsymbol{z} f) - f \operatorname{div} \boldsymbol{z}.$$

This leads to the ALE formulation of the Navier-Stokes equations

$$\frac{D^A \mathbf{w}}{Dt} + \sum_{s=1}^{2} \frac{\partial \boldsymbol{g}_s(\mathbf{w})}{\partial x_s} + \mathbf{w} \operatorname{div} \boldsymbol{z} = \sum_{s=1}^{2} \frac{\partial \boldsymbol{R}_s(\boldsymbol{w}, \nabla \boldsymbol{w})}{\partial x_s}, \tag{10}$$

where

$$\boldsymbol{g}_s(\mathbf{w}) := \boldsymbol{f}_s(\mathbf{w}) - z_s \mathbf{w}, \quad s = 1, 2,$$

are the ALE modified inviscid fluxes.

We see that in the ALE formulation of the Navier-Stokes equations the time derivative $\partial \boldsymbol{w}/\partial t$ is replaced by the ALE derivative $D^A \boldsymbol{w}/Dt$, the inviscid fluxes $\boldsymbol{f}_s$ are replaced by the ALE modified inviscid fluxes $\boldsymbol{g}_s$ and a new additional "'reaction"' term $\boldsymbol{w} \operatorname{div} \boldsymbol{z}$ appears.

## 3 Discrete problem

### 3.1 Discontinuous Galerkin space semidiscretization

For the space semidiscretization we use the discontinuous Galerkin finite element method. We construct a polygonal approximation $\Omega_{ht}$ of the domain $\Omega_t$. By $\mathcal{T}_{ht}$ we denote a partition of the closure $\overline{\Omega}_{ht}$ of the domain $\Omega_{ht}$ into a finite number of closed triangles $K$ with mutually disjoint interiors such that $\overline{\Omega}_{ht} = \bigcup_{K\in\mathcal{T}_{ht}} K$.

By $\mathcal{F}_{ht}$ we denote the system of all faces of all elements $K \in \mathcal{T}_{ht}$. Further, we introduce the set of all interior faces $\mathcal{F}^I_{ht} = \{\Gamma \in \mathcal{F}_{ht};\ \Gamma \subset \Omega_t\}$, the set of all boundary faces $\mathcal{F}^B_{ht} = \{\Gamma \in \mathcal{F}_{ht};\ \Gamma \subset \partial\Omega_{ht}\}$ and the set of all "Dirichlet" boundary faces $\mathcal{F}^D_{ht} = \left\{\Gamma \in \mathcal{F}^B_{ht};\ \text{a Dirichlet condition is prescribed on } \Gamma\right\}$. Each $\Gamma \in \mathcal{F}_{ht}$ is associated with a unit normal vector $\boldsymbol{n}_\Gamma$ to $\Gamma$. For $\Gamma \in \mathcal{F}^B_{ht}$ the normal $\boldsymbol{n}_\Gamma$ has the same orientation as the outer normal to $\partial\Omega_{ht}$. We set $d(\Gamma) =$ length of $\Gamma \in \mathcal{F}_{ht}$.

For each $\Gamma \in \mathcal{F}^I_{ht}$ there exist two neighbouring elements $K^{(L)}_\Gamma, K^{(R)}_\Gamma \in \mathcal{T}_h$ such that $\Gamma \subset \partial K^{(R)}_\Gamma \cap \partial K^{(L)}_\Gamma$. We use the convention that $K^{(R)}_\Gamma$ lies in the direction of $\boldsymbol{n}_\Gamma$ and $K^{(L)}_\Gamma$ lies in the opposite direction to $\boldsymbol{n}_\Gamma$. The elements $K^{(L)}_\Gamma$, $K^{(R)}_\Gamma$ are called neighbours. If $\Gamma \in \mathcal{F}^B_{ht}$, then the element adjacent to $\Gamma$ will be denoted by $K^{(L)}_\Gamma$.

The approximate solution will be sought in the space of discontinuous piecewise polynomial functions

$$\boldsymbol{S}_{ht} = [S_{ht}]^4, \quad \text{with} \quad S_{ht} = \{v; v|_K \in P_r(K)\ \forall\, K \in \mathcal{T}_{ht}\}, \tag{11}$$

where $r \geq 0$ is an integer and $P_r(K)$ denotes the space of all polynomials on $K$ of degree $\leq r$. A function $\boldsymbol{\varphi} \in \boldsymbol{S}_{ht}$ is, in general, discontinuous on interfaces $\Gamma \in \mathcal{F}^I_{ht}$. By $\boldsymbol{\varphi}^{(L)}_\Gamma$ and $\boldsymbol{\varphi}^{(R)}_\Gamma$ we denote the values of $\boldsymbol{\varphi}$ on $\Gamma$ considered from the interior and the exterior of $K^{(L)}_\Gamma$, respectively, and set

$$\langle\boldsymbol{\varphi}\rangle_\Gamma = (\boldsymbol{\varphi}^{(L)}_\Gamma + \boldsymbol{\varphi}^{(R)}_\Gamma)/2, \quad [\boldsymbol{\varphi}]_\Gamma = \boldsymbol{\varphi}^{(L)}_\Gamma - \boldsymbol{\varphi}^{(R)}_\Gamma. \tag{12}$$

The discrete problem is derived in the following way: We multiply system (10) by a test function $\boldsymbol{\varphi}_h \in \boldsymbol{S}_{ht}$, integrate over $K \in \mathcal{T}_{ht}$, use Green's theorem, sum over all elements $K \in \mathcal{T}_{ht}$, introduce the concept of the numerical flux and introduce suitable terms mutually vanishing for a regular exact solution. In this way we get the following identity:

$$\begin{aligned}\sum_{K\in\mathcal{T}_{ht}} \int_K \frac{D^A\boldsymbol{w}}{Dt} \cdot \boldsymbol{\varphi}_h\, dx + b_h(\boldsymbol{w},\boldsymbol{\varphi}_h) + a_h(\boldsymbol{w},\boldsymbol{\varphi}_h) + J_h(\boldsymbol{w},\boldsymbol{\varphi}_h) + d_h(\boldsymbol{w},\boldsymbol{\varphi}_h) \\ = \ell_h(\boldsymbol{w},\boldsymbol{\varphi}_h).\end{aligned} \tag{13}$$

Here

$$b_h(\boldsymbol{w},\boldsymbol{\varphi}_h) = -\sum_{K\in\mathcal{T}_{ht}}\int_K \sum_{s=1}^{2}\boldsymbol{g}_s(\boldsymbol{w})\cdot\frac{\partial\boldsymbol{\varphi}_h}{\partial x_s}\,dx \tag{14}$$
$$+\sum_{\Gamma\in\mathcal{F}_{ht}^I}\int_\Gamma \mathbf{H}_g(\boldsymbol{w}_\Gamma^{(L)},\boldsymbol{w}_\Gamma^{(R)},\boldsymbol{n}_\Gamma)\cdot[\boldsymbol{\varphi}_h]_\Gamma\,dS$$
$$+\sum_{\Gamma\in\mathcal{F}_{ht}^B}\int_\Gamma \mathbf{H}_g(\boldsymbol{w}_\Gamma^{(L)},\boldsymbol{w}_\Gamma^{(R)},\boldsymbol{n}_\Gamma)\cdot\boldsymbol{\varphi}_{h\Gamma}^{(L)}\,dS$$

is the convection form, defined with the aid of a numerical flux $\mathbf{H}_g$. We require that it is consistent with the fluxes $\boldsymbol{g}_s$: $\mathbf{H}_g(\boldsymbol{w},\boldsymbol{w},\boldsymbol{n}) = \sum_{s=1}^2 \boldsymbol{g}_s(\boldsymbol{w})n_s \quad (\boldsymbol{n}=(n_1,n_2), |\boldsymbol{n}|=1)$, conservative: $\mathbf{H}_g(\boldsymbol{u},\boldsymbol{w},\boldsymbol{n}) = -\mathbf{H}_g(\boldsymbol{w},\boldsymbol{u},-\boldsymbol{n})$, and locally Lipschitz-continuous.

Further, we define the viscous form

$$a_h(\boldsymbol{w},\boldsymbol{\varphi}_h) = \sum_{K\in\mathcal{T}_{ht}}\int_K \sum_{s=1}^{2}\mathbf{R}_s(\boldsymbol{w},\nabla\boldsymbol{w})\cdot\frac{\partial\boldsymbol{\varphi}_h}{\partial x_s}\,dx \tag{15}$$
$$-\sum_{\Gamma\in\mathcal{F}_{ht}^I}\int_\Gamma \sum_{s=1}^{2}\langle\mathbf{R}_s(\boldsymbol{w},\nabla\boldsymbol{w})\rangle_\Gamma(\boldsymbol{n}_\Gamma)_s\cdot[\boldsymbol{\varphi}_h]_\Gamma\,dS$$
$$-\sum_{\Gamma\in\mathcal{F}_{ht}^D}\int_\Gamma \sum_{s=1}^{2}\mathbf{R}_s(\boldsymbol{w},\nabla\boldsymbol{w})(\boldsymbol{n}_\Gamma)_s\cdot\boldsymbol{\varphi}_{h\Gamma}^{(L)}\,dS,$$

(we use the incomplete discretization of viscous terms - the so-called IIPG version), the interior and boundary penalty terms and the right-hand side form, respectively,

$$J_h(\boldsymbol{w},\boldsymbol{\varphi}_h) = \sum_{\Gamma\in\mathcal{F}_{ht}^I}\int_\Gamma \sigma[\boldsymbol{w}]_\Gamma\cdot[\boldsymbol{\varphi}_h]_\Gamma\,dS + \sum_{\Gamma\in\mathcal{F}_{ht}^D}\int_\Gamma \sigma\boldsymbol{w}\cdot\boldsymbol{\varphi}_{h\Gamma}^{(L)}\,dS, \tag{16}$$

$$\ell_h(\boldsymbol{w},\boldsymbol{\varphi}_h) = \sum_{\Gamma\in\mathcal{F}_{ht}^D}\int_\Gamma \sum_{s=1}^{2}\sigma\boldsymbol{w}_B\cdot\boldsymbol{\varphi}_{h\Gamma}^{(L)}\,dS. \tag{17}$$

Here $\sigma|_\Gamma = C_W\mu/d(\Gamma)$ and $C_W>0$ is a sufficiently large constant. The source form reads

$$d_h(\boldsymbol{w},\boldsymbol{\varphi}_h) = \sum_{K\in\mathcal{T}_{ht}}\int_K (\boldsymbol{w}\cdot\boldsymbol{\varphi}_h)\,\mathrm{div}\boldsymbol{z}\,dx. \tag{18}$$

The boundary state $\boldsymbol{w}_B$ is defined on the basis of the Dirichlet boundary conditions

and extrapolation:

$$\boldsymbol{w}_B = (\rho_D, \rho_D v_{D1}, \rho_D v_{D2}, c_v \rho_D \theta_\Gamma^{(L)} + \frac{1}{2}\rho_D |\boldsymbol{v}_D|^2) \quad \text{on } \Gamma_I, \tag{19}$$

$$\boldsymbol{w}_B = \boldsymbol{w}_\Gamma^{(L)} \quad \text{on } \Gamma_O, \tag{20}$$

$$\boldsymbol{w}_B = (\rho_\Gamma^{(L)}, \rho_\Gamma^{(L)} z_{D1}, \rho_\Gamma^{(L)} z_{D2}, c_v \rho_\Gamma^{(L)} \theta_\Gamma^{(L)} + \frac{1}{2}\rho_\Gamma^{(L)} |\boldsymbol{z}_D|^2) \quad \text{on } \Gamma_{W_t}. \tag{21}$$

The approximate solution is defined as $\boldsymbol{w}_h(t) \in \boldsymbol{S}_{ht}$ such that

$$\begin{aligned} \sum_{K \in \mathcal{T}_{ht}} \int_K \frac{D^A \boldsymbol{w}_h(t)}{Dt} \cdot \boldsymbol{\varphi}_h \, dx + b_h(\boldsymbol{w}_h(t), \boldsymbol{\varphi}_h) + a_h(\boldsymbol{w}_h(t), \boldsymbol{\varphi}_h) \\ + J_h(\boldsymbol{w}_h(t), \boldsymbol{\varphi}_h) + d_h(\boldsymbol{w}_h(t), \boldsymbol{\varphi}_h) = \ell_h(\boldsymbol{w}_h(t), \boldsymbol{\varphi}_h) \end{aligned} \tag{22}$$

holds for all $\boldsymbol{\varphi}_h \in \boldsymbol{S}_{ht}$, all $t \in (0, T)$ and $\boldsymbol{w}_h(0) = \boldsymbol{w}_h^0$ is an approximation of the initial state $\boldsymbol{w}^0$.

### 3.2 Time discretization

Let us construct a partition $0 = t_0 < t_1 < t_2 \ldots$ of the time interval $[0, T]$ and define the time step $\tau_k = t_{k+1} - t_k$. We use the approximations $\boldsymbol{w}_h(t_n) \approx \boldsymbol{w}_h^n \in \boldsymbol{S}_{ht_n}$, $\boldsymbol{z}(t_n) \approx \boldsymbol{z}^n$, $n = 0, 1, \ldots$ and introduce the function $\hat{\boldsymbol{w}}_h^k = \boldsymbol{w}_h^k \circ \mathcal{A}_{t_k} \circ \mathcal{A}_{t_{k+1}}^{-1}$, which is defined in the domain $\Omega_{ht_{k+1}}$. In order to approximate the ALE derivative at time $t_{k+1}$, we start from its definition and then use the backward difference:

$$\begin{aligned} \frac{D^A \boldsymbol{w}_h}{Dt}(x, t_{k+1}) &= \frac{\partial \tilde{\boldsymbol{w}}_h}{\partial t}(X, t_{k+1}) \\ &\approx \frac{\tilde{\boldsymbol{w}}_h^{k+1}(X) - \tilde{\boldsymbol{w}}_h^k(X)}{\tau_k} = \frac{\boldsymbol{w}_h^{k+1}(x) - \hat{\boldsymbol{w}}_h^k(x)}{\tau_k}, \qquad x = \mathcal{A}_{t_{k+1}}(X) \in \Omega_{ht_{k+1}}. \end{aligned} \tag{23}$$

By the symbol $(\cdot, \cdot)$ we shall denote the scalar product in $L^2(\Omega_{ht_{k+1}})$. A possible full discretization reads:

$$\begin{aligned} &\text{(a)} \quad \boldsymbol{w}_h^{k+1} \in \boldsymbol{S}_{ht_{k+1}}, \\ &\text{(b)} \quad \left( \frac{\boldsymbol{w}_h^{k+1} - \hat{\boldsymbol{w}}_h^k}{\tau_k}, \boldsymbol{\varphi}_h \right) + b_h(\boldsymbol{w}_h^{k+1}, \boldsymbol{\varphi}_h) + a_h(\boldsymbol{w}_h^{k+1}, \boldsymbol{\varphi}_h) \\ &\qquad + J_h(\boldsymbol{w}_h^{k+1}, \boldsymbol{\varphi}_h) + d_h\left(\boldsymbol{w}_h^{k+1}, \boldsymbol{\varphi}_h\right) = \ell_h(\boldsymbol{w}_h^{k+1}, \boldsymbol{\varphi}_h) \\ &\qquad \forall \boldsymbol{\varphi}_h \in \boldsymbol{S}_{ht_{k+1}}, \ k = 0, 1, \ldots. \end{aligned} \tag{24}$$

However, this problem for $\boldsymbol{w}_h^{k+1}$ is equivalent to a strongly nonlinear algebraic system and its solution is rather difficult.

Our goal is to develop a numerical scheme, which would be accurate and robust, with good stability properties and efficiently solvable. Therefore, we proceed similarly as in [7]

and use a partial linearization of the forms $b_h$ and $a_h$. This approach leads to a scheme that requires the solution of only one large sparse linear system on each time level.

The linearization of the first term of the form $b_h$ is based on the relations

$$\boldsymbol{g}_s(\boldsymbol{w}_h^{k+1}) = (\mathbb{A}_s(\boldsymbol{w}_h^{k+1}) - z_s^{k+1}\mathbb{I})\boldsymbol{w}_h^{k+1} \approx (\mathbb{A}_s(\hat{\boldsymbol{w}}_h^k) - z_s^{k+1}\mathbb{I})\boldsymbol{w}_h^{k+1},$$

where $\mathbb{A}_s(\mathbf{w})$ is the Jacobi matrix of $\boldsymbol{f}_s(\mathbf{w})$, cf. [10]. The second term of $b_h$ is linearized with the aid of the Vijayasundaram numerical flux (cf. [18]) defined in the following way. Taking into account the definition of $\boldsymbol{g}_s$, we have

$$\frac{D\boldsymbol{g}_s(\boldsymbol{w})}{D\boldsymbol{w}} = \frac{D\boldsymbol{f}_s(\boldsymbol{w})}{D\boldsymbol{w}} - z_s\mathbb{I} = \mathbb{A}_s - z_s\mathbb{I}, \tag{25}$$

and can write

$$\mathbb{P}_g(\boldsymbol{w}, \boldsymbol{n}) = \sum_{s=1}^{2} \frac{D\boldsymbol{g}_s(\boldsymbol{w})}{D\boldsymbol{w}} n_s = \sum_{s=1}^{2} (\mathbb{A}_s n_s - z_s n_s \mathbb{I}) \,. \tag{26}$$

By [10], this matrix is diagonalizable. It means that there exists a nonsingular matrix $\mathbb{T} = \mathbb{T}(\boldsymbol{w}, \boldsymbol{n})$ such that

$$\mathbb{P}_g = \mathbb{T}\mathbb{\Lambda}\mathbb{T}^{-1}, \quad \mathbb{\Lambda} = \mathrm{diag}(\lambda_1, \ldots, \lambda_4), \tag{27}$$

where $\lambda_i = \lambda_i(\boldsymbol{w}, \boldsymbol{n})$ are eigenvalues of the matrix $\mathbb{P}_g$. Now we define the "positive" and "negative" parts of the matrix $\mathbb{P}_g$ by

$$\mathbb{P}_g^{\pm} = \mathbb{T}\mathbb{\Lambda}^{\pm}\mathbb{T}^{-1}, \quad \mathbb{\Lambda}^{\pm} = \mathrm{diag}(\lambda_1^{\pm}, \ldots, \lambda_4^{\pm}), \tag{28}$$

where $\lambda^+ = \max(\lambda, 0)$, $\lambda^- = \min(\lambda, 0)$. Using the above concepts, we introduce the modified Vijayasundaram numerical flux (cf. [18] or [10]) as

$$\boldsymbol{H}_g(\boldsymbol{w}_L, \boldsymbol{w}_R, \boldsymbol{n}) = \tilde{\mathbb{P}}_g^+ \left( \frac{\boldsymbol{w}_L + \boldsymbol{w}_R}{2}, \boldsymbol{n} \right) \boldsymbol{w}_L + \tilde{\mathbb{P}}_g^- \left( \frac{\boldsymbol{w}_L + \boldsymbol{w}_R}{2}, \boldsymbol{n} \right) \boldsymbol{w}_R. \tag{29}$$

Using the above definition of the numerical flux, we introduce the approximations

$$\mathbf{H}_g(\boldsymbol{w}_{h\Gamma}^{k+1(L)}, \boldsymbol{w}_{h\Gamma}^{k+1(R)}, \boldsymbol{n}_\Gamma) \approx \mathbb{P}_g^+(\langle \hat{\boldsymbol{w}}_h^k \rangle_\Gamma, \boldsymbol{n}_\Gamma)\boldsymbol{w}_{h\Gamma}^{k+1(L)} + \mathbb{P}_g^-(\langle \hat{\boldsymbol{w}}_h^k \rangle_\Gamma, \boldsymbol{n}_\Gamma)\hat{\boldsymbol{w}}_{h\Gamma}^{k+1(R)}.$$

for $\Gamma \in \mathcal{F}_{ht_{k+1}}^I$ and

$$\mathbf{H}_g(\boldsymbol{w}_{h\Gamma}^{k+1(L)}, \boldsymbol{w}_{h\Gamma}^{k+1(R)}, \boldsymbol{n}_\Gamma) \approx \mathbb{P}_g^+(\langle \hat{\boldsymbol{w}}_h^k \rangle_\Gamma, \boldsymbol{n}_\Gamma)\boldsymbol{w}_{h\Gamma}^{k+1(L)} + \mathbb{P}_g^-(\langle \hat{\boldsymbol{w}}_h^k \rangle_\Gamma, \boldsymbol{n}_\Gamma)\hat{\boldsymbol{w}}_{h\Gamma}^{k(R)}.$$

for $\Gamma \in \mathcal{F}^B_{ht_{k+1}}$. In this way we get the form

$$\begin{aligned}
&\hat{b}_h(\hat{\boldsymbol{w}}_h^k, \boldsymbol{w}_h^{k+1}, \boldsymbol{\varphi}_h) \qquad (30)\\
&= -\sum_{K\in\mathcal{T}_{ht_{k+1}}} \int_K \sum_{s=1}^{2} (\mathbb{A}_s(\hat{\boldsymbol{w}}^k(x)) - z_s^{k+1}(x))\mathbb{I})\boldsymbol{w}^{k+1}(x)) \cdot \frac{\partial \boldsymbol{\varphi}_h(x)}{\partial x_s} dx,\\
&+ \sum_{\Gamma\in\mathcal{F}^I_{ht_{k+1}}} \int_\Gamma \Big(\mathbb{P}_g^+\big(\langle \hat{\boldsymbol{w}}_h^k\rangle, \boldsymbol{n}_\Gamma\big)\boldsymbol{w}_h^{k+1(L)} + \mathbb{P}_g^-\big(\langle \hat{\boldsymbol{w}}_h^k\rangle, \boldsymbol{n}_\Gamma\big)\boldsymbol{w}_h^{k+1(R)}\Big) \cdot [\boldsymbol{\varphi}_h] dS\\
&+ \sum_{\Gamma\in\mathcal{F}^B_{ht_{k+1}}} \int_\Gamma \Big(\mathbb{P}_g^+\big(\langle \hat{\boldsymbol{w}}_h^k\rangle, \boldsymbol{n}_\Gamma\big)\boldsymbol{w}_h^{k+1(L)} + \mathbb{P}_g^-\big(\langle \hat{\boldsymbol{w}}_h^k\rangle, \boldsymbol{n}_\Gamma\big)\hat{\boldsymbol{w}}_h^{k(R)}\Big) \cdot \boldsymbol{\varphi}_h dS.
\end{aligned}$$

The linearization of the form $a_h$ is based on the fact that $\mathbf{R}_s(\boldsymbol{w}_h, \nabla \boldsymbol{w}_h)$ is linear in $\nabla \boldsymbol{w}$ and nonlinear in $\boldsymbol{w}$. We get the linearized viscous form

$$\begin{aligned}
\hat{a}_h(\hat{\boldsymbol{w}}_h^k, \boldsymbol{w}_h^{k+1}, \boldsymbol{\varphi}_h) &= \sum_{K\in\mathcal{T}_{ht_{k+1}}} \int_K \sum_{s=1}^{2} \mathbf{R}_s(\hat{\boldsymbol{w}}_h^k, \nabla \boldsymbol{w}_h^{k+1}) \cdot \frac{\partial \boldsymbol{\varphi}_h}{\partial x_s}\, dx \qquad (31)\\
&- \sum_{\Gamma\in\mathcal{F}^I_{ht_{k+1}}} \int_\Gamma \sum_{s=1}^{2} \big\langle \mathbf{R}_s(\hat{\boldsymbol{w}}_h^k, \nabla \boldsymbol{w}^{k+1})\big\rangle (\boldsymbol{n}_\Gamma)_s \cdot [\boldsymbol{\varphi}_h]\, dS\\
&- \sum_{\Gamma\in\mathcal{F}^D_{ht_{k+1}}} \int_\Gamma \sum_{s=1}^{2} \mathbf{R}_s(\hat{\boldsymbol{w}}_h^k, \nabla \boldsymbol{w}_h^{k+1})(\boldsymbol{n}_\Gamma)_s \cdot \boldsymbol{\varphi}_h\, dS.
\end{aligned}$$

### 3.3 Artificial viscosity

In high-speed inviscid gas flow with large Mach numbers, discontinuities - called shock waves or contact discontinuities - appear. In viscous high-speed flow these discontinuities may be smeared due to viscosity and heat conduction. In both cases, near shock waves and contact discontinuities, the so-called Gibbs phenomenon, manifested by nonphysical spurious overshoots and undershoots, usually occurs in the numerical solution. In order to avoid this undesirable phenomenon, it is necessary to apply a suitable limiting procedure. Here we use the approach proposed in [11] based on the discontinuity indicator

$$g^k(K) = \int_{\partial K} [\hat{\rho}_h^k]^2 \,\mathrm{d}S \big/ (h_K |K|^{3/4}), \quad K \in \mathcal{T}_{ht_{k+1}}, \qquad (32)$$

introduced in [8]. By $[\hat{\rho}_h^h]$ we denote the jump of the function $\hat{\rho}_h^k$ on the boundary $\partial K$ and $|K|$ denotes the area of the element $K$. Then we define the discrete discontinuity indicator

$$G^k(K) = 0 \quad \text{if } g^k(K) < 1, \quad G^k(K) = 1 \quad \text{if } g^k(K) \geq 1, \quad K \in \mathcal{T}_{ht_{k+1}} \qquad (33)$$

and the artificial viscosity forms

$$\hat{\beta}_h(\hat{\boldsymbol{w}}_h^k, \boldsymbol{w}_h^{k+1}, \boldsymbol{\varphi}_h) = \nu_1 \sum_{K \in \mathcal{T}_{ht_{k+1}}} h_K G^k(K) \int_K \nabla \boldsymbol{w}_h^{k+1} \cdot \nabla \boldsymbol{\varphi}_h \, \mathrm{d}\boldsymbol{x} \tag{34}$$

and

$$\begin{aligned} &\hat{J}_h(\hat{\boldsymbol{w}}_h^k, \boldsymbol{w}_h^{k+1}, \boldsymbol{\varphi}_h) \\ &= \nu_2 \sum_{\Gamma \in \mathcal{F}^I_{ht_{k+1}}} \frac{1}{2}\big(G^k(K_\Gamma^{(L)}) + G^k(K_\Gamma^{(R)})\big) \int_\Gamma [\boldsymbol{w}_h^{k+1}] \cdot [\boldsymbol{\varphi}_h] \, \mathrm{d}\mathcal{S}, \end{aligned} \tag{35}$$

with parameters $\nu_1$, $\nu_2 = O(1)$.

Then the resulting scheme has the following form:

$$\begin{aligned} &\text{(a)} \quad \boldsymbol{w}_h^{k+1} \in \boldsymbol{S}_{ht_{k+1}}, \\ &\text{(b)} \quad \left(\frac{\boldsymbol{w}_h^{k+1} - \hat{\boldsymbol{w}}_h^k}{\tau_k}, \boldsymbol{\varphi}_h\right) \\ &\qquad + \hat{b}_h(\hat{\boldsymbol{w}}_h^k, \boldsymbol{w}_h^{k+1}, \boldsymbol{\varphi}_h) + \hat{a}_h(\hat{\boldsymbol{w}}_h^k, \boldsymbol{w}_h^{k+1}, \boldsymbol{\varphi}_h) \\ &\qquad + J_h(\boldsymbol{w}_h^{k+1}, \boldsymbol{\varphi}_h) + d_h\left(\boldsymbol{w}_h^{k+1}, \boldsymbol{\varphi}_h\right) \\ &\qquad + \hat{\beta}_h(\hat{\boldsymbol{w}}_h^k, \boldsymbol{w}_h^{k+1}, \boldsymbol{\varphi}_h) + \hat{J}_h(\hat{\boldsymbol{w}}_h^k, \boldsymbol{w}_h^{k+1}, \boldsymbol{\varphi}_h) = \ell(\boldsymbol{w}_B^k, \boldsymbol{\varphi}) \\ &\qquad \forall \boldsymbol{\varphi}_h \in \boldsymbol{S}_{ht_{k+1}}, \ k = 0, 1, \ldots. \end{aligned} \tag{36}$$

This method successfully overcomes problems with the Gibbs phenomenon in the context of the semi-implicit scheme. It is important that the indicator $G^k(K)$ vanishes in regions, where the solution is regular and, therefore, the numerical solution does not contain any nonphysical entropy production in these regions.

### 3.4 Treatment of boundary states in the form $\hat{b}_h$

If $\Gamma \in \mathcal{F}^B_{ht_{k+1}}$, it is necessary to specify the boundary state $\hat{\boldsymbol{w}}_{h\Gamma}^{k(R)}$ appearing in the numerical flux $\boldsymbol{H}_g$ in the definition of the inviscid form $\hat{b}_h$. For simplicity we shall use the notation $\boldsymbol{w}^{(R)}$ for values of the function $\hat{\boldsymbol{w}}_{h\Gamma}^{k(R)}$ which should be determined at individuals integration points on the face $\Gamma$. Similarly, $\boldsymbol{w}^{(L)}$ will denote the values of $\hat{\boldsymbol{w}}_{h\Gamma}^{k(L)}$ at the corresponding points.

On the inlet, which is assumed fixed, we proceed in the same way as in [11], Section 4. Using the rotational invariance, we transform the Euler equations

$$\frac{\partial \boldsymbol{w}}{\partial t} + \sum_{s=1}^{2} \frac{\partial \boldsymbol{f}_s(\boldsymbol{w})}{\partial x_s} = 0$$

to the coordinates $\tilde{x}_1$, parallel with the normal direction $\boldsymbol{n} = (n_1, n_2) = \boldsymbol{n}_\Gamma$ to the boundary, and $\tilde{x}_2$, tangential to the boundary, neglect the derivative with respect to $\tilde{x}_2$ and linearize the system around the state $\boldsymbol{q}^{(L)} = \boldsymbol{Q}(\boldsymbol{n})\boldsymbol{w}^{(L)}$, where

$$\boldsymbol{Q}(\boldsymbol{n}) = \begin{pmatrix} 1, & 0, & 0, & 0 \\ 0, & n_1, & n_2, & 0 \\ 0, & -n_2, & n_1, & 0 \\ 0, & 0, & 0, & 1 \end{pmatrix} \tag{37}$$

is the rotational matrix. Then we obtain the linear system

$$\frac{\partial \boldsymbol{q}}{\partial t} + \mathbb{A}_1(\boldsymbol{q}^{(L)})\frac{\partial \boldsymbol{q}}{\partial \tilde{x}_1} = 0, \tag{38}$$

for the transformed vector-valued function $\boldsymbol{q} = \boldsymbol{Q}(\boldsymbol{n})\boldsymbol{w}$, considered in the set $(-\infty, 0) \times (0, \infty)$ and equipped with the initial and boundary conditions

$$\boldsymbol{q}(\tilde{x}_1, 0) = \boldsymbol{q}^{(L)},\ \tilde{x}_1 < 0, \quad \text{and} \quad \boldsymbol{q}(0, t) = \boldsymbol{q}^{(R)},\ t > 0. \tag{39}$$

The goal is to choose $\boldsymbol{q}^{(R)}$ in such a way that this initial-boundary value problem is well posed, i.e. has a unique solution. The method of characteristics leads to the following process:

Let us put $\boldsymbol{q}^* = \boldsymbol{Q}(\boldsymbol{n})\boldsymbol{w}^*$, where $\boldsymbol{w}^*$ is a given boundary state at the inlet or outlet. We calculate the eigenvectors $\boldsymbol{r}_s$ corresponding to the eigenvalues $\lambda_s,\ s = 1, \dots, 4$, of the matrix $\mathbb{A}_1(\boldsymbol{q}^{(L)})$, arrange them as columns in the matrix $\mathbb{T}$ and calculate $\mathbb{T}^{-1}$. Now we set

$$\boldsymbol{\alpha} = \mathbb{T}^{-1}\boldsymbol{q}^{(L)}, \quad \boldsymbol{\beta} = \mathbb{T}^{-1}\boldsymbol{q}^* \tag{40}$$

and define the state $\boldsymbol{q}^{(R)}$ by the relations

$$\boldsymbol{q}^{(R)} := \sum_{s=1}^{4} \gamma_s \boldsymbol{r}_s, \quad \gamma_s = \begin{cases} \alpha_s, & \lambda_s \geq 0, \\ \beta_s, & \lambda_s < 0. \end{cases} \tag{41}$$

Finally, the sought boundary state $\boldsymbol{w}^{(R)}$ is defined as

$$\boldsymbol{w}^{(R)} = \boldsymbol{Q}^{-1}(\boldsymbol{n})\boldsymbol{q}^{(R)}. \tag{42}$$

On the impermeable moving wall we prescribe the normal component of the velocity

$$\boldsymbol{v} \cdot \boldsymbol{n} = \boldsymbol{z}_D \cdot \boldsymbol{n}, \tag{43}$$

where $\boldsymbol{n}$ is the unit outer normal to $\Gamma_{W_t}$ and $\boldsymbol{z}_D$ is the wall velocity. This means that two eigenvalues of $\mathbb{P}_g(\boldsymbol{w}, \boldsymbol{n})$ vanish, one is positive and one is negative. Then, in analogy to [10], Section 3.3.6, we should prescribe one quantity, namely $\boldsymbol{v} \cdot \boldsymbol{n}$, and extrapolate three quantities - tangential velocity, density and pressure.

However, here we define the numerical flux on $\Gamma_{W_t}$ as the physical flux through the boundary with the assumption (43) taken into account. Thus, on $\Gamma_{W_t}$ we write

$$\sum_{s=1}^{2} \boldsymbol{g}_s(\boldsymbol{w}) n_s = (\boldsymbol{v}\cdot\boldsymbol{n} - \boldsymbol{z}_D\cdot\boldsymbol{n})\boldsymbol{w} + p\,(0, n_1, n_2, \boldsymbol{v}\cdot\boldsymbol{n})^T \tag{44}$$
$$= p\,(0, n_1, n_2, \boldsymbol{z}_D\cdot\boldsymbol{n})^T =: \boldsymbol{H}_g.$$

As another possibility of the treatment of the boundary conditions on a solid wall one could use a suitable adaptation of the approach proposed in [12].

On the outlet (which does not depend on time) the pressure is prescribed and other variables are extrapolated. However, it will be necessary to pay a special attention to the treatment of the outlet boundary conditions in order to avoid a reflection of vortices, which sometimes appears.

**Remark 1.** *In practical computations, integrals appearing in the definitions of the forms* $\hat{a}_h$, $\hat{b}_h$, ... *are evaluated with the aid of quadrature formulas.*

*The developed numerical scheme can also be used for the numerical solution of inviscid flow, if we set* $\mu = \lambda = k = 0$. *See [11].*

*The linear algebraic system equivalent to (37), b) is solved either by a direct solver UMFPACK ([4]) or by the GMRES method with block diagonal preconditioning.*

## 4 Numerical experiments

In order to demonstrate the applicability of the developed method, we present here results of some numerical experiments.

I) We consider inviscid compressible flow in the rectangular channel with the initial shape $\Omega_0 = [-2, 2] \times [0, 1]$, where the lower wall of the channel is moving. The ALE mapping is equal to identity in the sets $[-2, -1] \times [0, 1]$ and $[1, 2] \times [0, 1]$. In the rest of the channel we construct the ALE mapping so that the lower wall is represented at time $t$ by the graph of the function

$$0.45\sin(0.4t)\,(\cos(\pi X_1) + 1),\ \ X_1 \in (-1, 1). \tag{45}$$

This movement is interpolated to the rest of the domain resulting in the ALE mapping $\mathcal{A}_t$ (see [14]). The computation was carried out with the dimensionless form of the Euler equations, using the dimensionless conservation variables, on a triangulation with 1160 elements constructed by the technique from [5]. The inlet Mach number $M_{inlet} = 0.067$, the dimensionless inlet density $\rho_{inlet} = 1.0$. At the outlet, the dimensionless pressure $p_{outlet} = 159.12$. In the artificial viscosity forms (34) and (35) the values $\nu_1 = \nu_2 = 0.2$ were used.

Figure 1 shows velocity and pressure isolines at different time instants $t = 0.3992$, 2.2192, 4.1792, 7.1192, 13.9792, 14.9592. In the solution we can observe a vortex formation, when the lower wall starts to descend. This vortex is convected through the domain.

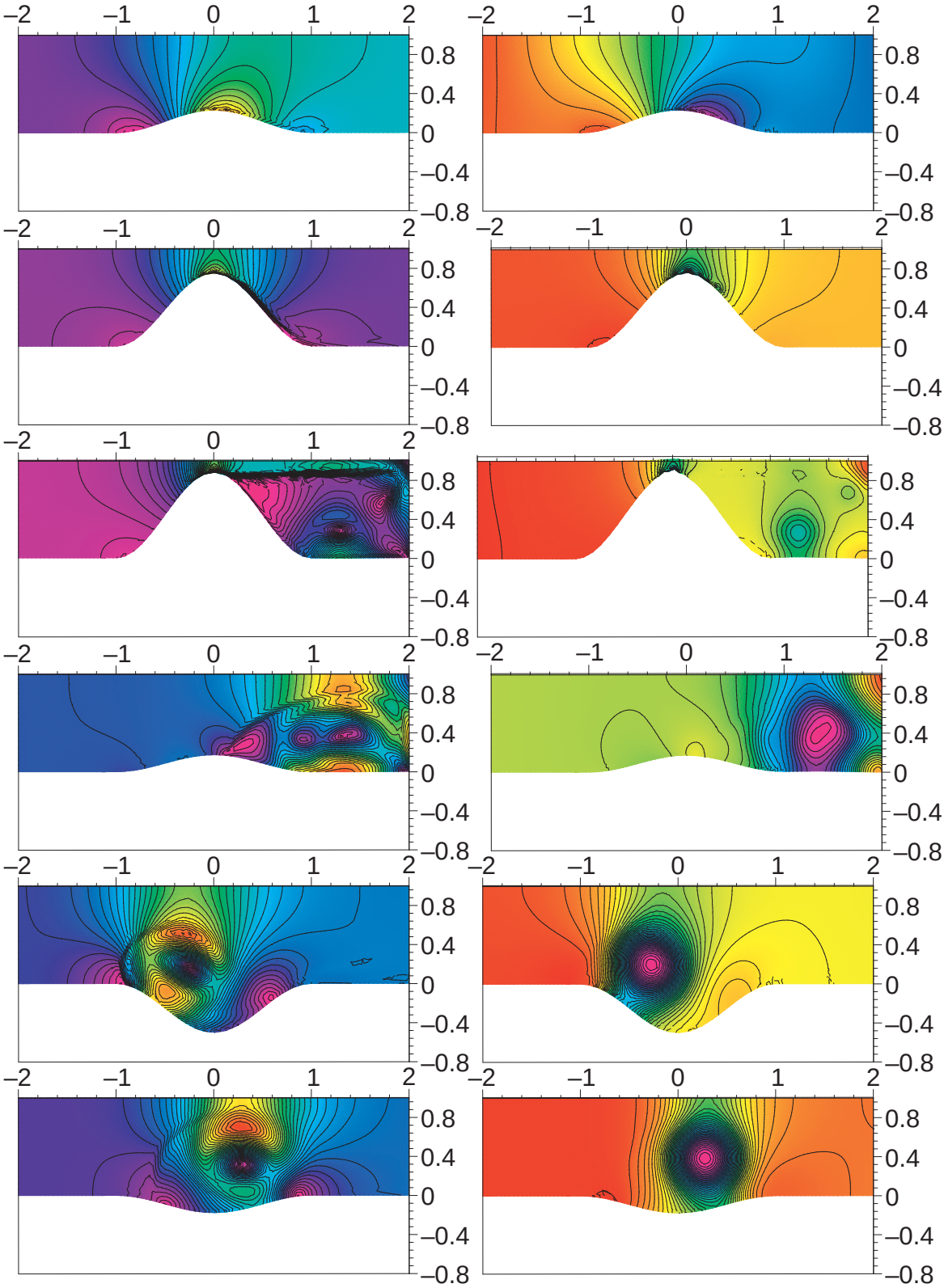


Figure 1: Velocity (left) and pressure (right) isolines at time instants $t = 0.3992$, 2.2192, 4.1792, 7.1192, 13.9792, 14.9592.

Moreover, we see that a contact discontinuity is developed, when the channel becomes narrow. The contact discontinuity is characterized by the discontinuity in the velocity, whereas the pressure remains continuous.

II) In the second example we present results of numerical experiments carried out for viscous compressible flow in a channel with geometry from [15] inspired by the shape of the human glottis and a part of supraglottal spaces as shown in Figure 2. The walls are moving in order to mimic the vibrations of vocal folds during voice production. The lower channel wall between the points A and B and the upper wall symmetric with respect to the axis of the channel are vibrating up and down periodically with frequency 100 Hz. This movement is interpolated into the domain resulting in the ALE mapping $\mathcal{A}_t$.

The width of the channel at the inlet (left part of the boundary) is $H = 0.016$ m and its length is $L = 0.16$ m. The width of the narrowest part of the channel (at the point C) oscillates between 0.0004 m and 0.0028 m. We consider the following input parameters and boundary conditions: magnitude of the inlet velocity $v_{in} = 4$ m/s, the viscosity $\mu = 15 \cdot 10^{-6}\ \mathrm{kg\,m^{-1}\,s^{-1}}$, the inlet density $\rho_{in} = 1.225\ \mathrm{kg\,m^{-3}}$, the outlet pressure $p_{out} = 97611$ Pa, the Reynolds number $Re = \rho_{in} v_{in} H/\mu = 5227$, heat conduction coefficient $k = 2.428 \cdot 10^{-2}\,\mathrm{kg\,m\,s^{-2}\,K^{-1}}$, the specific heat $c_v = 721.428\,\mathrm{m^2\,s^{-2}\,K^{-1}}$, the Poisson adiabatic constant $\gamma = 1.4$. The inlet Mach number is $M_{in} = 0.012$. In the numerical tests, piecewise quadratic elements ($r = 2$) are used.

Figure 3 shows computed streamlines and velocity at different dimensionless time instants $t = 502.5$, 544.5, 586.5, 628.5 during the fourth period of the motion. In the solution we can observe large vortex formation convected through the domain. The flow field is neither periodic, nor axisymmetric, in spite the computational domain is axisymmetric and the motion of the channel walls is periodic and symmetric as well. Figure 4 shows the details of flow near the vocal folds corresponding to dimensionless time instants 517.5, 567, 616.5, 666, 715.5 and 765.

III) Finally, the last example is concerned with the simulation of vibrations of elastically supported airfoil NACA 0012 induced by compressible viscous flow. The airfoil has two degrees of freedom: the vertical displacement $H$ (positively oriented downwards) and the angle of rotation around an elastic axis $\alpha$ (positively oriented clockwise). The motion of the airfoil is described by the system of nonlinear ordinary differential equations for

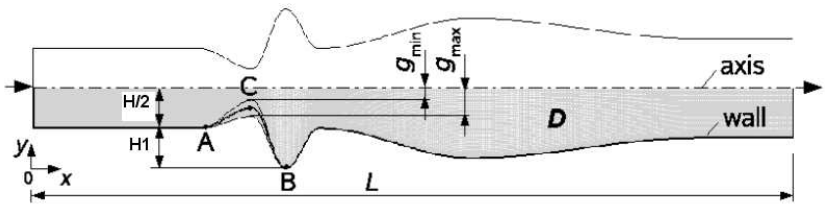


Figure 2: Computational domain (cf. [15]).

unknowns $H, \alpha$:

$$m\ddot{H} + k_{HH}H + S_\alpha\,\ddot{\alpha}\,\cos\alpha - S_\alpha\dot{\alpha}^2\sin\alpha + d_{HH}\dot{H} = -L(t), \tag{46}$$
$$S_\alpha\ddot{H}\cos\alpha + I_\alpha\ddot{\alpha} + k_{\alpha\alpha}\alpha + d_{\alpha\alpha}\dot{\alpha} = M(t).$$

We use the the following notation: $L(t)$ - aerodynamic lift force (upwards positive), $M(t)$ - aerodynamic torsional moment (clockwise positive), $m$ - mass of the airfoil, $S_\alpha$ - static moment around the elastic axis EO, $I_\alpha$ - inertia moment around the elastic axis EO, $k_{HH}$ - bending stiffness, $k_{\alpha\alpha}$ - torsional stiffness, $d_{HH}$ - structural damping in bending, $d_{\alpha\alpha}$ - structural damping in torsion, $c$ - length of the chord of the airfoil, $l$ - airfoil depth.

System (46) is equipped with the initial conditions prescribing the values $h(0), \alpha(0)$, $\dot{h}(0), \dot{\alpha}(0)$. It is transformed to first-order ODE systems and solved numerically by the fourth-order Runge-Kutta method. For the derivation of equations (46), see [16]. The aerodynamic lift force $L$ acting in the vertical direction and the torsional moment $M$ are defined by

$$L = -\,l\int_{\Gamma_{Wt}}\sum_{j=1}^{2}\tau_{2j}n_j dS, \quad M = l\int_{\Gamma_{Wt}}\sum_{i,j=1}^{2}\tau_{ij}n_j r_i^{\mathrm{ort}} dS, \tag{47}$$

where

$$\tau_{ij} = (-p + \lambda\,\mathrm{div}\boldsymbol{v})\delta_{ij} + \mu\left(\frac{\partial u_i}{\partial x_j} + \frac{\partial u_j}{\partial x_i}\right), \tag{48}$$
$$r_1^{\mathrm{ort}} = -(x_2 - x_{EO2}),\ r_2^{\mathrm{ort}} = x_1 - x_{EO1}.$$

By $\tau_{ij}$ we denote the components of the stress tensor, $\delta_{ij}$ denotes the Kronecker symbol, $\boldsymbol{n} = (n_1, n_2)$ is the unit outer normal to $\partial\Omega_t$ on $\Gamma_{Wt}$ (pointing into the airfoil) and $x_{EO} = (x_{EO1}, x_{EO2})$ is the position of the elastic axis (lying in the interior of the airfoil). Relations (47) and (48) define the coupling of the fluid dynamical model with the structural model.

The simulation of flow induced airfoil vibrations was carried out for the following data: $m = 0.086622$ kg, $S_a = -0.000779673$ kg m, $I_a = 0.000487291$ kg m$^{-2}$, $k_{HH} =$ N/m, $k\alpha\alpha = 3.696682$ Nm/rad, $l = 0.05$ m, $c = 0.3$ m, $\mu = 1.8375 \cdot 10^{-5}$ kg m$^{-1}$ s$^{-1}$, far-field density $\rho = 1.225$ kg m$^{-3}$, $H(0) = 0.02$, m, $\alpha(0) = 6$ degrees, $\dot{H}(0) = 0, \dot{\alpha} = 0$. We neglect the structural damping. The elastic axis is placed on the airfoil chord at the 40% distance from the leading edge.

The computational process starts at time $t = 0$ by the solution of the flow, keeping the airfoil in a fixed position given by the prescribed initial translation $H$ and the angle of attack $\alpha$. Then, at some time $t > 0$ the airfoil is released and we continue by the solution of a complete fluid-structure interaction problem.

Figure 5 shows the displacement $H$ and the rotation angle $\alpha$ in dependence on time for the far-field velocity 30, 35 and 40 m/s. We see that for the velocities 30 and 35 m/s the vibrations are damped, but for the velocity 40 m/s we get the flutter instability when the vibration amplitudes are increasing in time. The monotonous increase and decrease of the average values of $H$ and $\alpha$, respectively, shows that the flutter is combined with a divergence instability in the presented example.

## 5 Conclusion

We have presented an efficient higher-order numerical scheme for the solution of the compressible Euler or Navier-Stokes equations in time dependent domains and the simulation of flow induced airfoil vibrations. It is based on several important ingredients:

- the ALE method applied to the compressible Euler and Navier-Stokes equations,
- the application of the discontinuous Galerkin method for the space discretization,
- semi-implicit time discretization,
- special treatment of boundary conditions,
- artificial viscosity applied in the vicinity of discontinuities.

The presented method behaves as unconditionally stable and appears to be robust with respect to the magnitude of the Mach number. Future work will be concentrated on the following topics:

- further analysis of various treatments of boundary conditions,
- the realization of a remeshing in case of closing the channel during the oscillation period of the channel walls,
- the coupling of the developed method with the solution of elasticity equations describing the deformation of vocal folds,
- the use of a suitable turbulence model.

## REFERENCES

[1] F. Bassi and S. Rebay, High-order accurate discontinuous finite element solution of the 2D Euler equations, *J. Comput. Phys.*, **138**, 251–285 (1997).

[2] C. E. Baumann and J. T. Oden, A discontinuous *hp* finite element method for the Euler and Navier-Stokes equations, *Int. J. Numer. Methods Fluids*, **31**, 79–95 (1999).

[3] B. Cockburn, G. E. Karniadakis and C.-W. Shu (Eds.), Discontinuous Galerkin methods, Lecture Notes in Computational Science and Engineering 11, *Springer* (2000).

[4] T. A. Davis and I. S. Duff, A combined unifrontal/multifrontal method for unsymmetric sparse matrices, *ACM Transactions on Mathematical Software*, **25**, 1–19 (1999).

[5] V. Dolejší, Anisotropic mesh adaptation for finite volume and finite element methods on triangular meshes, *Comput. Vis. Sci.*, **1**(3), 165–178 (1998).

[6] V. Dolejší: Semi-implicit interior penalty discontinuous Galerkin methods for viscous compressible flows. *Commun. Comput. Phys.*, **4**, 231–274 (2008).

[7] V. Dolejší and M. Feistauer, A semi-implicit discontinuous Galerkin finite element method for the numerical solution of inviscid compressible flow, *J. Comput. Phys.*, **198**, 727–746 (2004).

[8] V. Dolejší, M. Feistauer and C. Schwab, On some aspects of the discontinuous Galerkin finite element method for conservation laws, *Math. Comput. Simul.*, **61**, 333–346 (2003).

[9] M. Feistauer, V. Dolejší and V. Kučera, On the discontinuous Galerkin method for the simulation of compressible flow with wide range of Mach numbers, *Computing and Visualization in Science*, **10**, 17–27 (2007).

[10] M. Feistauer, J. Felcman and I. Straškaraba, Mathematical and Computational Methods for Compressible Flow, *Clarendon Press*, Oxford (2003).

[11] M. Feistauer and V. Kučera, On a robust discontinuous Galerkin technique for the solution of compressible flow, *J. Comput. Phys.*, **224**, 208–221 (2007).

[12] L. Krivodonova and M. Berger, High-order accurate implementation of solid wall boundary conditions in curved geometries, *J. Comput. Phys.* **211**, 492–512 (2006).

[13] T. Nomura and T.J.R. Hughes, An arbitrary Lagrangian-Eulerian finite element method for interaction of fluid and a rigid body, *Comput. Methods Appl. Mech. Engrg.*, **95**, 115-138 (1992).

[14] J. Prokopová, Numerical solution of compressible flow, Master thesis, *Charles University*, Prague, (2008).

[15] P. Punčochářová, J. Fürst, K. Kozel and J. Horáček, Numerical solution of compressible flow with low Mach number through oscillating glottis, In Proceedings of the *9th International Conference On Flow-Induced Vibration (FIV 2008)*, I Zolotarev, J. Horáček Eds., *Institute of Thermomechanics AS CR*, Prague, 135-140 (2008).

[16] P. Sváček, M. Feistauer and J. Horáček, Numerical simulation of flow induced airfoil vibrations with large amplitudes. *J. of Fluids and Structures*, **23**, 391-411 (2007).

[17] J. J. W. van der Vegt and H. van der Ven, Space-time discontinuous Galerkin finite element method with dynamic grid motion for inviscid compressible flow, *J. Comput. Phys.*, **182**, 546–585 (2002).

[18] G. Vijayasundaram, Transonic flow simulation using upstream centered scheme of Godunov type in finite elements, *J. Comput. Phys.*, **63**, 416–433 (1086).

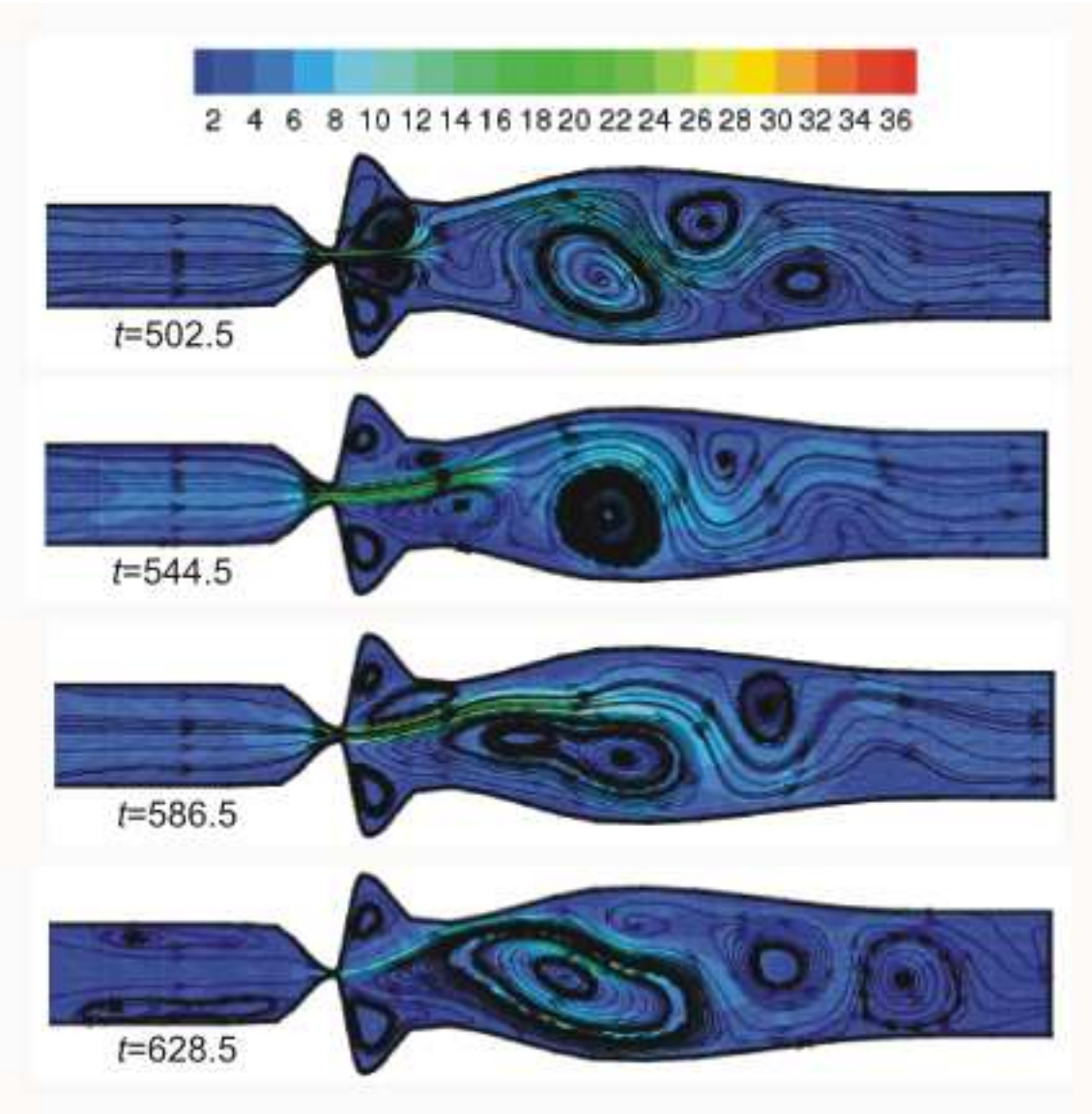


Figure 3: Streamlines and velocity at dimensionless time instants $t = 502.5$, 544.5, 586.5, 628.5.

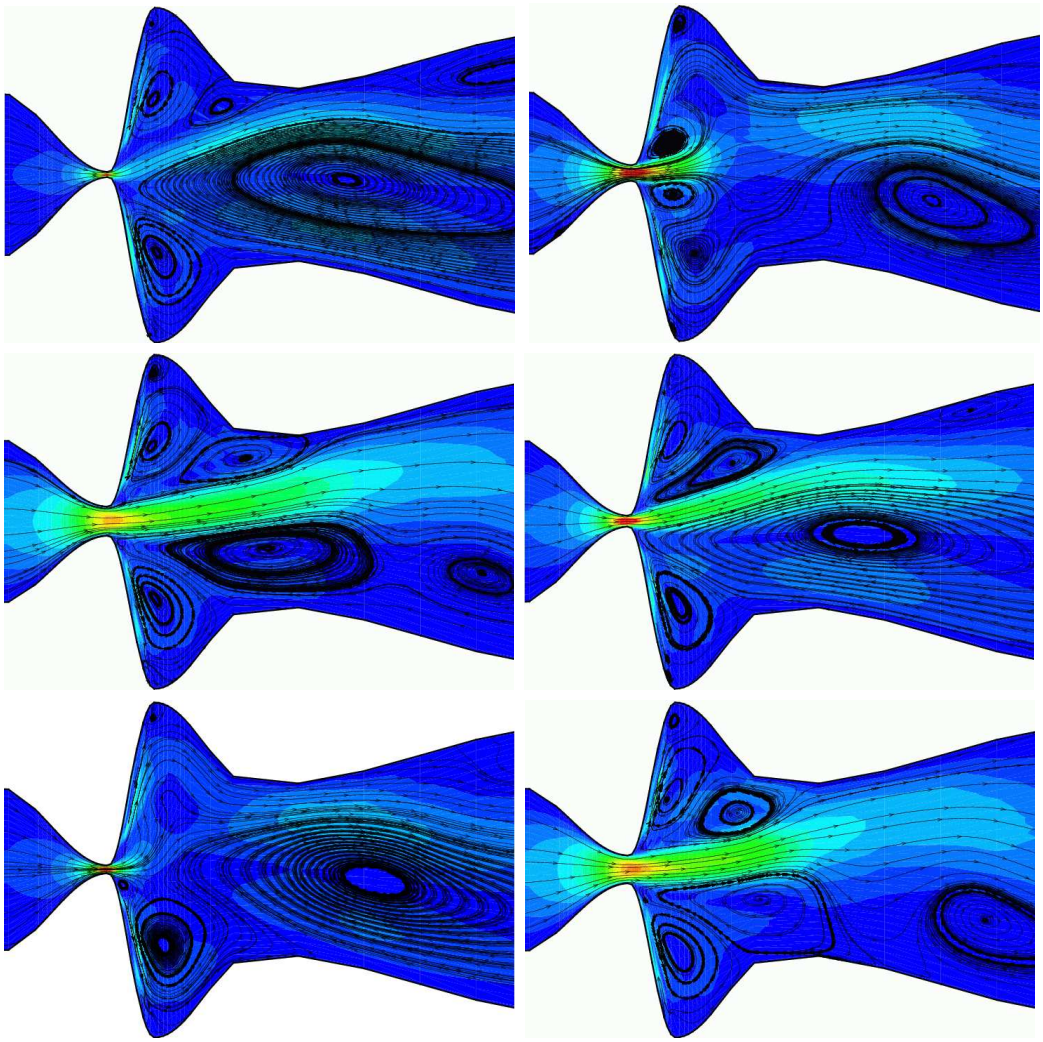

Figure 4: Detail of the flow near the vocal folds - visualization of the velocity and streamlines at dimensionless time instants 517.5, 567, 616.5, 666, 715.5 and 765.

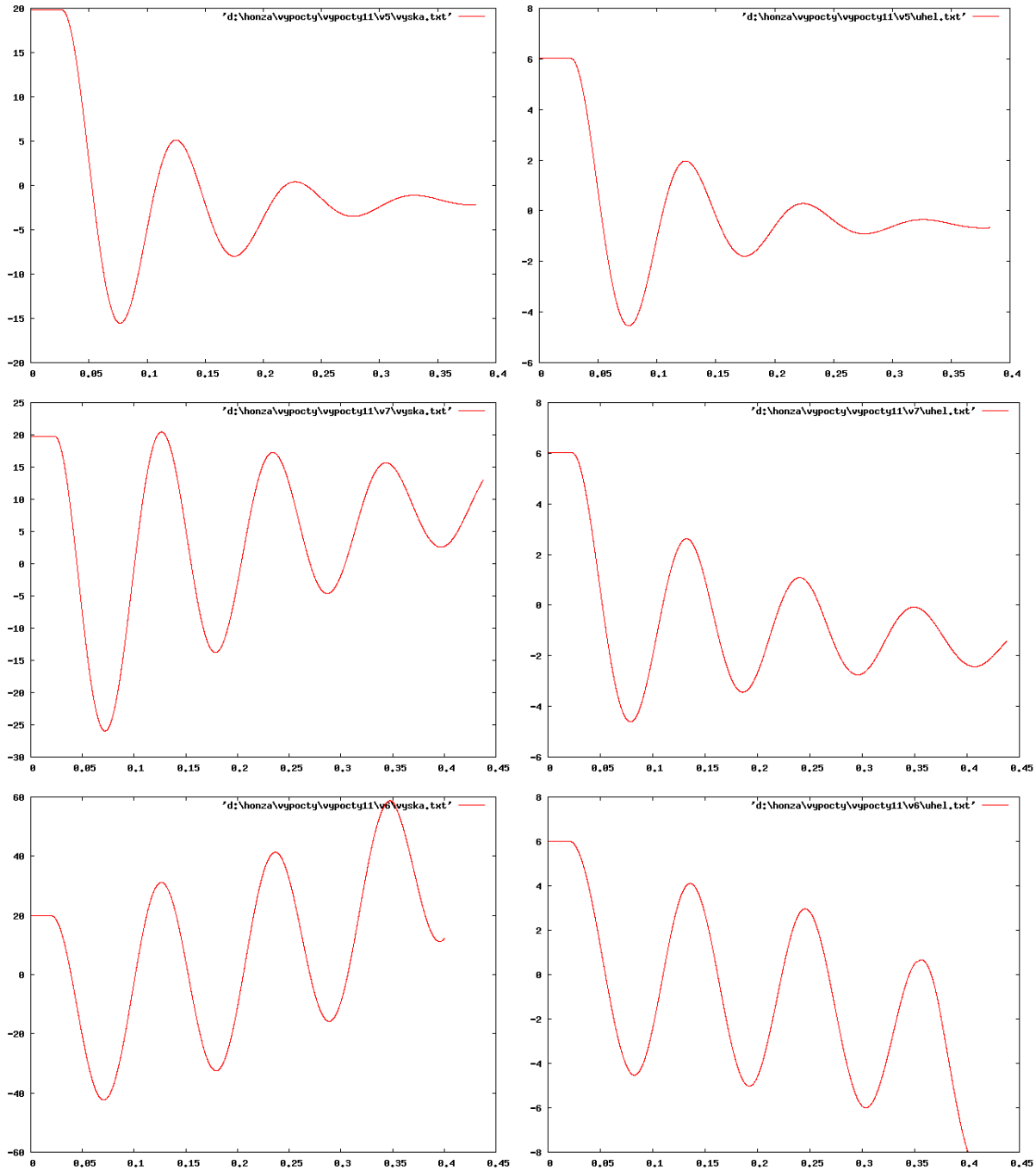


Figure 5: Displacement $H$ (left) and rotation angle $\alpha$ (right) of the airfoil in dependence on time for far-field velocity 30, 35 and 40 m/s.